*Progress In Electromagnetics Research C, Vol. 54, 57–66, 2014*

# A Wideband and High Gain Dual-Polarzied Antenna Design by a Frequency-Selective Surface for WLAN Application

**Hua Zhu[1, 2, 3], Yang Yu[1, 2, 3], Xiuping Li[1, 2, 3, *], and Bo Ai[3]**

**Abstract**—A new dual-polarized antenna loading frequency-selective surface (FSS) is proposed for 5G wireless local networks (WLANs) application. The antenna consists of two orthogonal bow-tie dipoles and a ground plane. A new wideband FSS is designed comprising ring-slot connecting rectangular slots. The reflection coefficient of wideband FSS is less than 0.9 from 4–6.5 GHz. The phase of reflection coefficient is $-163°$ at 5.5 GHz. The novel cell analyzed by the equivalent circuit is given and simulated. The wideband FSS is employed as a superstrate layer for bandwidth enhancement and radiation gain improvement of the antenna. After loading wideband FSS, the measured bandwidth is 5.3–6.3 GHz (17.2%) with $S_{11}$ and $S_{22}$ both less than $-10$ dB, which cover various 5G WLAN bandwidths. The gain of the antenna is 12.1 dBi at 5.5 GHz. The bandwidth of antenna with FSS increases 40%, and gain improves 5.6 dBi. The simulated and measured results agree well.

## 1. INTRODUCTION

At present, the demand of wireless local area networks (WLANs) is increasing greatly worldwide for commercial and industrial communications because WLAN provides high speed connectivity and easy access to networks without wiring. Antennas with dual-polarized radiation characteristics have been very attractive to base-station antenna designs for WLAN [1–4] applications. The dual-polarized antennas retain considerable advantage of combating complex propagation of the transmit/receive waves in the WLAN environment [5]. In addition, polarization sensitivity of the antenna is mitigated by utilizing the dual-polarized antennas. These features certainly benefit wireless access points (APs) or routers in practical applications [6]. However, the tremendous growth of wireless communication services results in increasing demand for wideband and high-gain antennas with stringent electrical characteristics.

To meet these requirements, various types of antennas have been studied to develop WLAN antennas, operating at 5-GHz band. Several techniques for bandwidth enhancement, dual-polarization and low polarization have been proposed [7–12]. In [7, 8], aperture-coupled patch antennas with modified coupling slots are designed for achieving dual-polarization radiation with high isolation over a wide bandwidth. However, they all have the disadvantages of high cross-polarization levels because of the transverse currents of the higher-order modes. In [9], two pairs of T-shaped slots on the two bow-tie shaped patches excited by two coax-line feeds are designed to low cross polarization and high port isolation. But the size is large. In [11], an orthogonal coupling feed antenna is designed. Stacked directors are designed for high gain. However, the gain is increased less. Dual-polarized MIMO WLAN antenna arrays have been developed [13, 14]. A MIMO array is obtained in a triangular configuration at 5.2 GHz band [13]. Moreover, a dual-band dual-polarized compact bow-tie dipole antenna array is designed for MIMO WLAN, which supports beam switching [14].

*Received 28 July 2014, Accepted 23 September 2014, Scheduled 13 October 2014*

* Corresponding author: Xiuping Li (xpli@bupt.edu.cn).

[1] School of Electronic Engineering, University of Posts and Telecommunications, Beijing, China. [2] Beijing Key Laboratory of Work Safety Intelligent Monitoring (Beijing University of Posts and Telecommunications), Beijing 100876, China. [3] State Key Laboratory of Rail Traffic Control and Safety, Beijing Jiaotong University, China.

In recent years, FSS has been widely studied, which possesses the capability of increasing gain and broadening bandwidth [15–21]. One of the most important challenges in the design of the antenna loading FSS is its frequency bandwidth for the return loss and maximum directivity. These characteristics depend on FSS layer and feed source. In most works, a suitable FSS is designed to achieve wideband and high gain [22–24]. In [22], a FSS layer with square loop elements is proposed as the antenna's superstrate layer for achieving wide bandwidth and increased directivity. The FSS layer has $9 \times 9$ elements. The bandwidth of FSS has increased about 5% and directivity increased about 70%. In [23], a new triple-band FSS is designed and composed of three conductor-based split-ring resonators connected together. The proposed antenna operates in 8.6, 10 and 11.2 GHz, respectively. Gain of the antenna with FSS has been improved by 2.5 dBi.

In this paper, an antenna for wideband and high-gain operation using two orthogonal bow-tie dipoles as the feeding source and an FSS wideband structure as the superstrate layer for high directivity is proposed. Two orthogonal bow-tie dipoles are designed for dual-polarization. For wideband, the FSS with ring-slot connecting rectangular slots is designed. The novel cell analyzed by the equivalent circuit is given and simulated. The antennas with and without loading FSS are simulated and measured. Both simulated and measured results agree well.

This paper is organized as follows. Section 2 presents the wideband FSS structure. The proposed FSS structure and its equivalent circuit model are also discussed. Section 3 presents the dual-polarized antenna loading FSS is studied. Simulated and measured results are given. Section 4 presents the analysis with verified key Parameters.

## 2. WIDEBAND FSS DESIGN

Antenna is placed between ground plane and FSS as shown in Fig. 1. The structure is based on the formation of an open resonant cavity between the ground plane and FSS that acts as a partially reflective surface (PRS). Near its resonance frequency where the reflection coefficient of surface is about unity, the radiating source and FSS layer produce resonance condition in which the directivity of the antenna increases considerably [25, 26]. The resonant cavity antenna achieves a maximum directivity $D_{\max}$ as follows [27, 28]:

$$D_{\max} = \frac{1 + \left|Re^{j\varphi}\right|}{1 - \left|Re^{j\varphi}\right|} \tag{1}$$

where $R$ is the reflection magnitude of FSS and $\varphi$ the reflection phase of FSS. $h$ is determined by:

$$-\pi + \varphi - 4\pi h/\lambda_0 = 2N\pi, \quad N = 0, \pm 1, \pm 2, \ldots \tag{2}$$

where $-\pi$ is the reflection phase of the ground plane. For a highly reflective FSS ($R \approx 1$ and $\varphi \approx \pi$), a high directivity $D_{\max}$ is obtained, and the resonant distance is $h \approx \lambda/2$ (for $N = 1$). High reflectivity values are obtained for a wide range of frequencies. Moreover, the slow variation of reflection phase contributes toward a good bandwidth performance for the antenna.

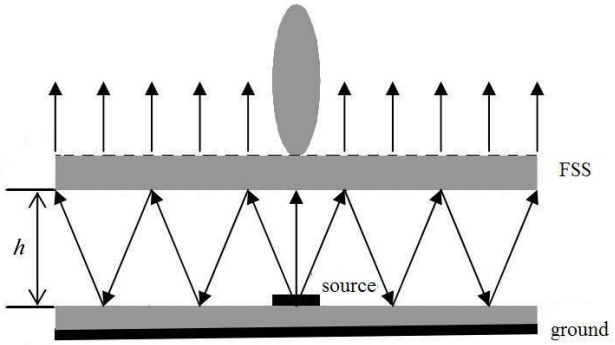


**Figure 1.** Resonant cavity antenna formed by ground plane and FSS.

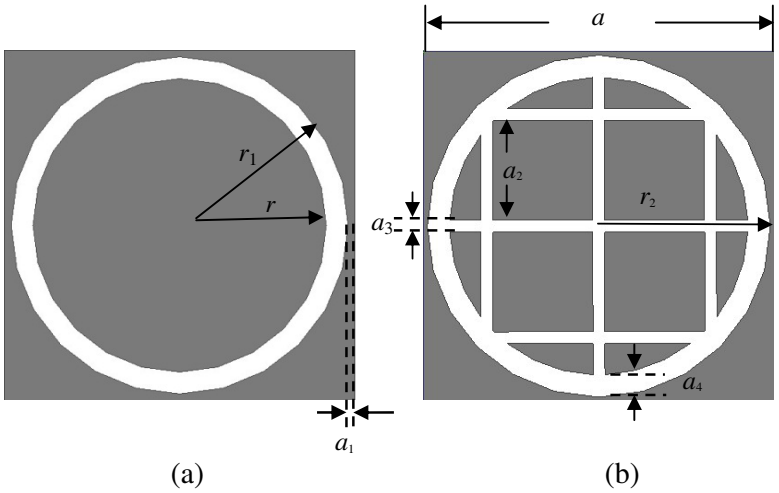


**Figure 2.** Evolution of the proposed FSS structure. (a) FSS-A with circular slot. (b) FSS-B with circular slot and rectangular slots.

Figure 2 shows the evolution steps of the proposed wideband FSS structure. We start with the circular slot (FSS-A) with dimensional variables as shown in Fig. 2(a). The metallic circular patch arranged periodically is positioned at center of a wire grid. The radii of circular patch and wire grid are $r$ and $r_1$. In the next step, we introduce six regular slots as shown in Fig. 2(b). This can be regarded as parallel multiple resonator $LC$ circuits of the structure. The two kinds of FSS are placed on a FR-4 substrate (relative permittivity $\varepsilon = 4.4$, $\tan\delta = 0.02$, $H = 1.6\,\text{mm}$). The optimized parameters are shown in Table 1.

The equivalent circuit model of FSS-A is depicted in Fig. 3(a). From Fig. 3(a), the circular patch

**Table 1.** Parameter for the FSS (mm).

| Parameters | Values | Parameters | Values |
|---|---|---|---|
| $a$ | 23.5 | $r$ | 7.5 |
| $a_1$ | 0.5 | $r_1$ | 10 |
| $a_2$ | 6 | $r_2$ | 11 |
| $a_3$ | 1 | $a_4$ | 1.5 |

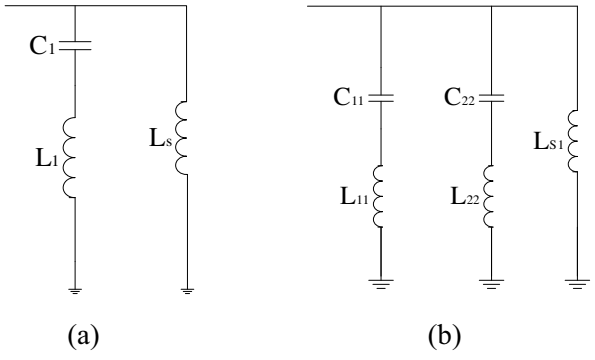


**Figure 3.** Equivalent circuit model of the designed FSS. (a) FSS-A with circular slot. (b) FSS-B with circular slot and rectangular slots.

**Table 2.** Electrical parameter for the FSS.

| Electrical parameter | Values | Electrical parameter | Values |
|---|---|---|---|
| $C_1$ | 0.6 pF | $L_s$ | 6 nH |
| $C_{11}$ | 1 pF | $L_{s1}$ | 6 nH |
| $C_{22}$ | 0.8 pF | $R_1$ | 1.5 Ω |
| $L_1$ | 1.5 nH | $R_2$ | 1 Ω |
| $L_{11}$ | 0.5 nH | $R_3$ | 1 Ω |
| $L_{22}$ | 0.8 nH | | |

acts as $L_1C_1$ resonator. The wire grid acts as inductors ($L_s$) that are parallel with the $L_1C_1$ resonator. The structure's impedance can be found as follows [29]:

$$Z_{FSS\text{-}A} = jwL_s \frac{1-\omega^2 L_1 C_1}{1-\omega^2(L_1+L_s)C_1} \tag{3}$$

The resonant frequency of FSS-A can be found as follows:

$$f_r = \frac{1}{2\pi\sqrt{\varepsilon_r(L_1+L_s)\cdot C_1}} \tag{4}$$

The bandwidth of FSS-A can be expressed by (5)

$$BW = \frac{\pi}{8\eta_0}\sqrt{\frac{L_1+L_s}{C_1}} \times \left(\frac{L_s}{L_1+L_s}\right) \tag{5}$$

It is evident from (5) that FSS-A structure can be enhanced by increasing the inductance $L_1$ or decreasing capacitance $C_1$. Introduction of six regular slots at the center loads FSS-A with the series $L_{11}C_{11}$ resonator and the parallel $L_{22}C_{22}$ resonator. Fig. 3(b) shows the simplified equivalent circuit model of the designed FSS-B. The impedance of FSS-B can be found as follows:

$$Z_{FSS\text{-}B} = jwL_{s1} \frac{\left(1-\omega^2 L_{11}C_{11}\right)\left(1-\omega^2 L_{22}C_{22}\right)}{\omega^4 L_{11}L_{22}C_{11}C_{22} - \omega^2 C_{11}(L_{11}+L_{s1}) - \omega^2 C_{22}(L_{22}+L_{s1}) + 1} \tag{6}$$

The resonance frequency of the equivalent circuit can be obtained from a quadratic

$$\omega^4 L_{11}L_{22}C_{11}C_{22} - \omega^2 C_{11}(L_{11}+L_{s1}) - \omega^2 C_{22}(L_{22}+L_{s1}) + 1 = 0 \tag{7}$$

The electrical parameters are shown in Table 2. The HFSS model and ADS circuit model is used to compute the reflection magnitude and phase characteristics of FSS-A and FSS-B depicted in Fig. 4. The magnitude of reflection coefficient of FSS-A is less than 0.7 from 4–6.5 GHz. The phase of reflection coefficient is $-163°$ at 5.5 GHz. The phase of reflection coefficient changes from $-163°$ to $-130°$ in bandwidth. The magnitude of reflection coefficient of FSS-B is less than 0.9 from 4–6.5 GHz. The phase of reflection is $-163°$ at 5.5 GHz. The phase of reflection changes from $-170°$ to $-155°$ in bandwidth. It is seen that the magnitude of reflection coefficient of FSS-B is close to 1, and the phase of reflection coefficient has slow variation within the bandwidth, compared to FSS-A.

## 3. ANTENNA WITH FSS DESIGN

The geometry of the antenna with FSS is shown in Fig. 5(a). It is composed of three sections including dual-polarized antenna, FSS superstrate layer and ground. The dual-polarized antenna consists of two bow-tie shape dipoles, a Balun for feeding port and ground, as shown in Fig. 5(b). Two bow-tie shaped dipoles are placed in the vertical slots to achieve dual-polarization. The bow-tie shaped dipoles and the square ground are printed on the top side of the FR4 substrate (relative permittivity $\varepsilon_r = 4.4$, $\tan\delta = 0.02$, $H = 1.6$ mm). Two feeding lines are printed on the bottom side. Both antenna strips are on the front side perpendicularly connected to the ground. The balun connects the dipole strip by a via-hole on back side. The feeding line and balun is connected by plugs through the ground board.

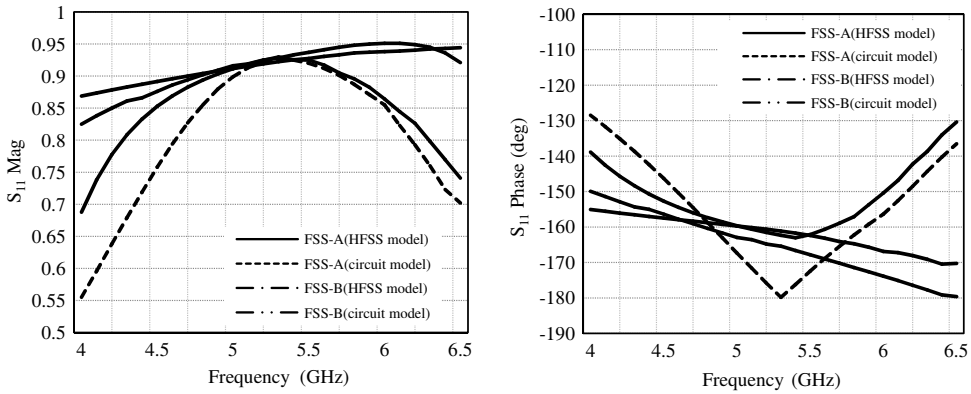


**Figure 4.** Simulated magnitude and phase of reflection coefficient. (a) FSS-A. (b) FSS-B.

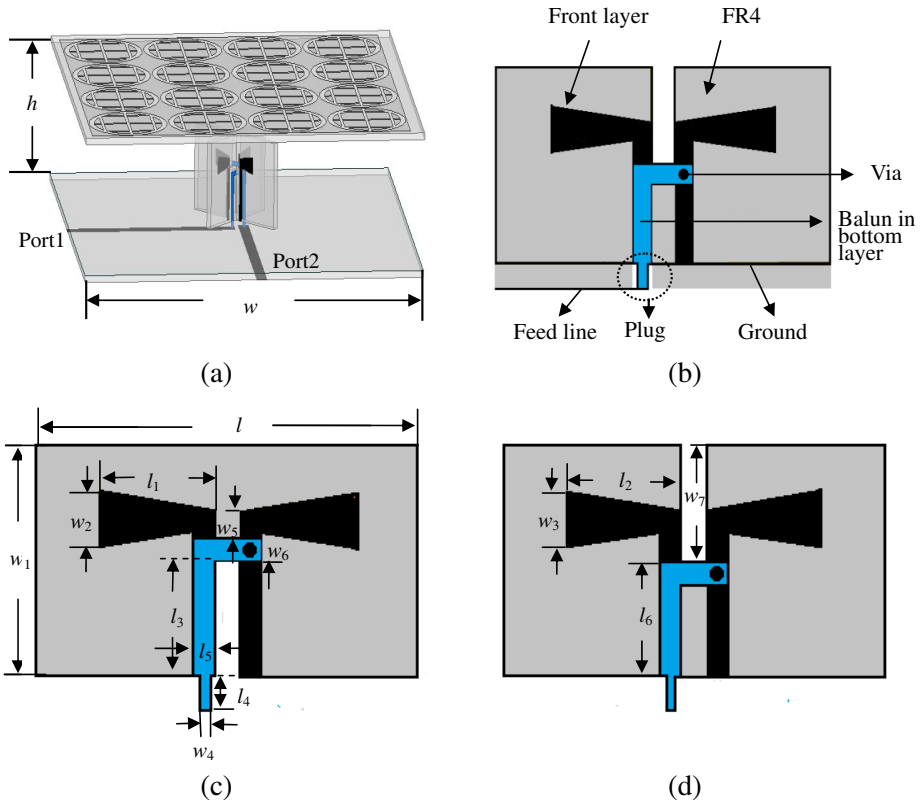


**Figure 5.** Geometry of antenna with FSS. (a) 3D view of antenna loading FSS. (b) Antenna board configuration. (c) Element type 1. (d) Element type 2.

The proposed antenna with FSS is fabricated. A photograph is shown in Fig. 6. The FSS with $4 \times 4$ elements is located on top of the antenna surface with a distance of $h$. The size is $106 \times 106 \times 35.2\,\text{mm}^3$. The optimized parameters are shown in Table 3.

The simulated results from HFSS are shown in Fig. 7. It is observed that the simulated bandwidth of without FSS is around 0.6 GHz (5.5 $\sim$ 6.1 GHz) under the condition of voltage standing wave ratio (VSWR) less than 2. The simulated bandwidth of antenna with FSS is around 1.3 GHz (5.2 $\sim$ 6.5 GHz) under the condition of VSWR less than 2. The measured bandwidth of antenna with FSS is around 1 GHz (5.3 $\sim$ 6.3 GHz) under the condition of VSWR less than 2.The simulated and measured results agree well. It is observed that the bandwidth increases 40%.

**Figure 6.** Photographs of the fabricated antenna with FSS.

**Table 3.** Parameter for the antenna element (mm).

| Parameters | Values | Parameters | Values |
|---|---|---|---|
| $l$ | 20 | $w$ | 106 |
| $l_1$ | 5.5 | $w_1$ | 20 |
| $l_2$ | 5 | $w_2$ | 4 |
| $l_3$ | 10 | $w_3$ | 4 |
| $l_4$ | 1 | $w_4$ | 1 |
| $l_5$ | 2 | $w_5$ | 1 |
| $l_6$ | 12.5 | $w_6$ | 2 |
| $h$ | 33 | $w_7$ | 8 |

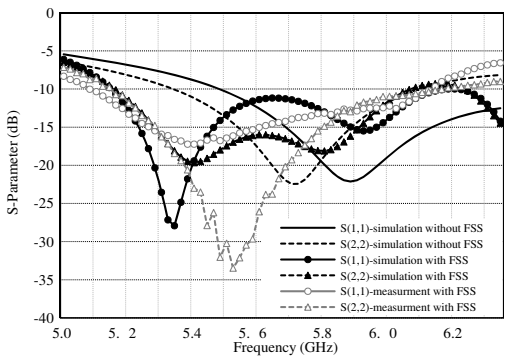


**Figure 7.** Comparison of $S_{11}/S_{22}$ with and without FSS structure.

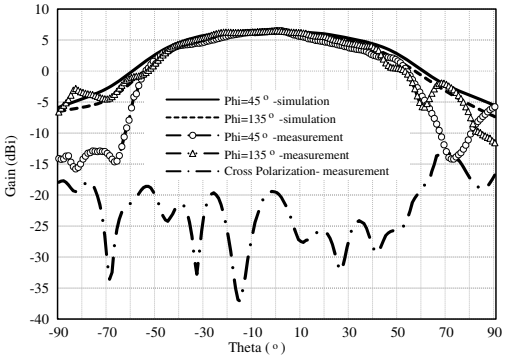


**Figure 8.** The simulated and measured gain results of the antenna without FSS at 5.5 GHz.

The simulated and measured gains of the antenna without FSS are shown in Fig. 8. The simulated maximum gain is 6.3 dBi. The half-power beam width is 95°. The measured maximum gain is 6.5 dBi. The half-power beam width is 85°. The measured cross polarization in the main beam direction (theta = 0°) is suppressed by −19 dB. The simulated and measured results agree well.

The simulated and measured gains of the antenna with FSS are shown in Fig. 9. The simulated maximum gain is 13.2 dBi. The half-power beam width is 34°. The measured maximum gain is 12.1 dBi. The half-power beam width is 38°. The measured cross polarization in the main beam direction (theta = 0°) is suppressed by −25 dB. The simulated and measured results agree well.

The simulated gain with frequency is shown in Fig. 10. In the band of 5–6 GHz, the simulated gain of antenna without FSS changes from 6.7 to 5.9 dBi. In the band of 5–6 GHz, the simulated gain of antenna with FSS changes from 10 to 13.2 dBi. The gain of antenna with FSS has been improved about 5.6 dBi, compared to the antenna without FSS.

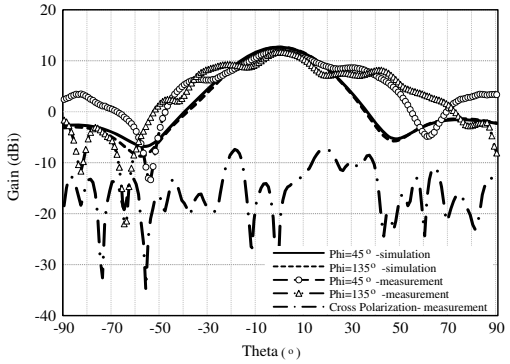


**Figure 9.** The simulated and measured gain results of the antenna with FSS at 5.5 GHz.

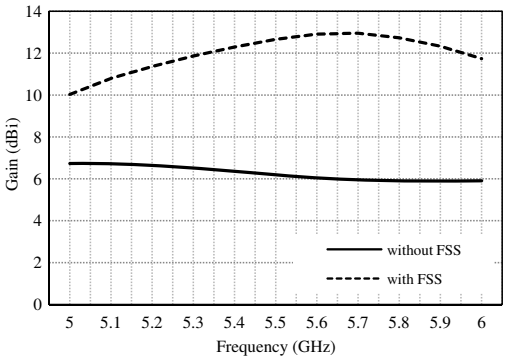


**Figure 10.** The gain with frequency.

## 4. PARAMETERS ANALYSIS

The effects of important parameters such as the height and dimensions of the FSS layer are studied.The effects of varying the height of the FSS are shown in Fig. 11. When $h$ is increased from 32.5 to 33.5 mm, the bandwidth increases 140 MHz on the high frequency, as shown in Fig. 11(a). The gain moves from 12.5 dBi to 13.5 dBi, and the maximum gain moves to lower frequency, as shown in Fig. 11(b).

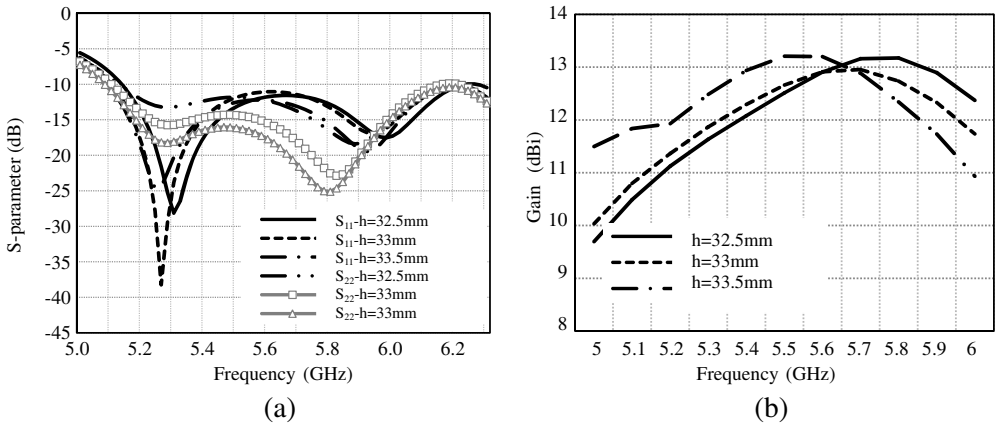


**Figure 11.** Effect of the FSS height. (a) $S$-parameter. (b) Gain.

Another important parameter in the design of antenna with FSS is the FSS dimensions. The antenna is considered the leaky waves propagating toward the edges of FSS and producing radiating current distribution on the FSS layer. Increasing the dimensions of FSS layer leads to the increase of the radiating aperture of the antenna. In the antenna constructed using the FSS surface, the leakage current is tapered toward the edges of the FSS [30, 31]. Therefore, the dimensions of the FSS superstrate layer must be chosen.

To examine the effects of the FSS dimensions, the FSS superstrate layer is studied with different numbers of elements. Fig. 12 depicts $s$-parameter and gain of the antenna for the FSS with different numbers of elements. Simulation results show that enhancing the dimension of FSS more than $6 \times 6$ elements, the bandwidth increases 220 MHz on the high frequency, as shown in Fig. 12(a). The gain improves 0.8 dBi, and the maximum gain moves to lower frequency, as shown in Fig. 12(b).

Figure 13 shows the surface current on the FSS superstrate layer which produces the radiating Fields. The FSS superstrate layer has $4 \times 4$ elements. As it is seen, this current is tapered toward the edges of the cavity. For our design the surface current focuses on in the middle of the FSS.

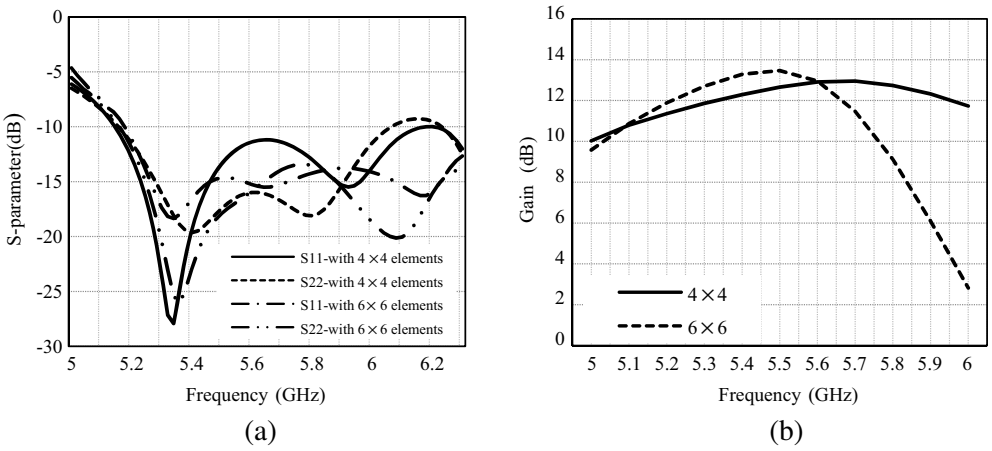


**Figure 12.** Effect of the FSS with different elements number. (a) $S$-parameter. (b) Gain.

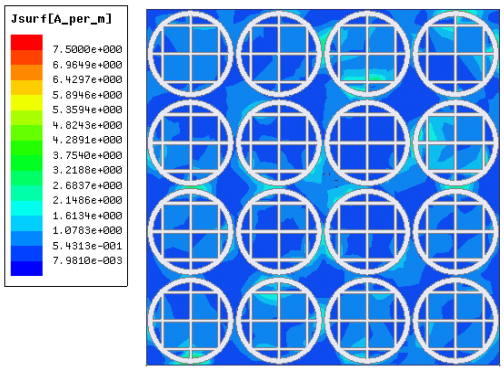


**Figure 13.** Current distribution on the FSS surface of antenna.

## 5. CONCLUSION

A new dual-polarized antenna loading FSS for 5G wireless local networks (WLANs) application is proposed in this paper. To obtain the dual-polarization, the antenna consists of two orthogonal bow-tie dipoles and a ground plane. A new wideband FSS is designed comprising ring-slot connecting rectangular slots. The FSS is employed as a superstrate layer for bandwidth enhancement and radiation gain improvement of antenna. After loading FSS, the simulation and measured bandwidth is around 5.3–6.3 GHz (17.2%) with $S_{11}$ and $S_{22}$ less than $-10$ dB, which covers various 5G WLAN bandwidths. The gain of the antenna is 12.1 dBi at 5.5 GHz. The antenna with FSS increases 40%, and gain improves 5.6 dBi. The simulated and measured results agree well.

## ACKNOWLEDGMENT

This work is supported by the project 61072009 and 61372036 from the National Natural Science Foundation of China (NSFC), Fundamental Research Funds for the Central Universities and the State Key Laboratory of Rail Traffic Control and Safety (Contract No. RCS2014K002), BeijingJiaotong University.

## REFERENCES

1. See, T. S. P. and Z. N. Chen, "Design of dual-polarization stackedarrays for ISM band applications," *Microw. Opt. Technol. Lett.*, Vol. 38, 142–147, Jul. 2003.

2. Chang, F. S., H. T. Chen, K. C. Chao, and K. L. Wong, "Dual-polarized probe-fed patch antenna with highly decoupled ports for WLAN basestation," *IEEE Antennas Propag. Soc. Int. Symp. Dig.*, 101–109, Monterey, CA, USA, 2004.
3. Guo, Y. X. and K. M. Luk, "Dual-polarized dielectric resonator antennas," *IEEE Transactions on Antennas and Propagation*, Vol. 51, 1120–1124, May 2003.
4. Su, S.-W. and C.-T. Lee, "Printed, low-cost, dual-polarized dual-loop-antenna system for 2.4/5 GHz WLAN access points," *Proceedings of the 5th European Conference Antennas and Propagation (EUCAP)*, 1253–1257, 2011.
5. Zheng, W. C., L. Zhang, Q. X. Li, and Y. Leng, "Dual-band dual-polarized compact bowtie antenna array for anti-interference MIMO WLAN," *IEEE Transactions on Antennas and Propagation*, Vol. 62, No. 1, 237–246, Jan. 2014.
6. Su, S.-W. and C.-T. Lee, "Printed, low-cost, dual-polarized dual-loop-antenna system for 2.4/5 GHz WLAN access points," *IEEE Transactions on Antennas and Propagation*, Vol. 59, No. 5, 1653–1659, May 2011.
7. Wong, K. L., H. C. Tung, and T. W. Chiou, "Broadband dual-polarize daperture-coupled patch antennas with modified H-shaped coupling slots," *IEEE Transactions on Antennas and Propagation*, Vol. 50, No. 2, 188–191, Feb. 2002.
8. Gao, S. C., L. W. Li, M. S. Leong, and T. S. Yeo, "Dual-polarized slot coupled planar antenna with wide bandwidth," *IEEE Transactions on Antennas and Propagation*, Vol. 51, No. 3, 441–448, Mar. 2003.
9. Li, B., Y.-Z. Yin, W. Hu, Y. Ding, and Y. Zhao, "Wideband dual-polarized patch antenna with low cross polarization and high isolation," *IEEE Antennas and Wireless Propagation Letters*, Vol. 11, 427–429, 2012.
10. Kaboli, M., S. A. Mirtaheri, and M. S. Abrishamian, "High-isolation X-polar antenna," *IEEE Antennas and Wireless Propagation Letters*, Vol. 9, 401–404, 2010.
11. Jia, T. and X. Li, "A compact stacked bidirectional antenna for dual-polarized WLAN applications," *Progress In Electromagnetics Research C*, Vol. 44, 95–108, 2013.
12. Moghadas, H. and M. Daneshmand, "Dual-band dual-polarized high-gain resonant cavity antenna," *IEEE International Symposium Antennas and Propagation (APSURSI)*, 2246–2249, 2011.
13. Capobianco, A., F. M. Pigozzo, A. Assalini, M. Midrio, S. Boscolo, and F. Sacchetto, "A compact MIMO array of planar end-fire antennas for WLAN applications," *IEEE Transactions on Antennas and Propagation*, Vol. 59, No. 9, 3462–3465, Sep. 2011.
14. Chuang, H.-R. and L.-C. Kuo, "3-D FDTD design analysis of a 2.4-GHz polarization-diversity printed dipole antenna with integrated balun and polarization-switching circuit for WLAN and wireless communication applications," *IEEE Trans. Microwave Theory and Technique*, Vol. 51, 374–381, 2003.
15. Cook, B. S. and A. Shamim, "Utilizing wideband AMC structures for high-gain inkjet-printed antennas on lossy paper substrate," *IEEE Antennas and Wireless Propagation Letters*, Vol. 12, 76–79, 2013.
16. Kim, D., "Novel dual-band Fabry-Perot cavity antenna with low frequency separation ratio," *Microw. Opt. Technol. Lett.*, Vol. 51, No. 8, 1869–1872, Aug. 2009.
17. Sauleau, R. and P. Coquet, "Input impedance of electromagnetic bandgap resonator antennas," *Microw. Opt. Technol. Lett.*, Vol. 41, No. 5, 369–375, Jun. 2004.
18. Rodes, E., M. Diblanc, E. Arnaud, T. Monediere, and B. Jecko, "Dual-band EBG resonator antenna using a single-layer FSS," *IEEE Antennas and Wireless Propagation Letters*, Vol. 6, 368–371, 2007.
19. Wu, Z.-H. and W.-X. Zhang, "Broadband printed compound air-fed array antennas," *IEEE Antennas and Wireless Propagation Letters*, Vol. 9, 187–190, 2010.
20. Almeida Filho, V. A. and A. L. P. de Siqueira Campos, "Performance optimization of microstrip antenna array using frequency selective surfaces," *J. Microw. Optoelectron. Electromagn. Appl.*, Vol. 13, No. 1, 31–46, 2014.

21. Brito, D. B., A. G. d'Assunção, R. H. C. Maniçoba, and X. Begaud, "Metamaterial inspired fabry-pérot antenna with cascaded frequency selective surfaces," *Microw. Opt. Technol. Lett.*, Vol. 55, 981–985, 2013.
22. Pirhadi, A., H. Bahrami, and J. Nasri, "Wideband high directive aperture coupled microstrip antenna design by using a FSS superstrate layer," *IEEE Transactions on Antennas and Propagation*, Vol. 60, No. 4, 2101–2106, Apr. 2012.
23. Moharamzadeh, E. and A. M. Javan, "Triple-band frequency-selective surfaces to enhance gain of X-band triangle slot antenna," *IEEE Antennas and Wireless Propagation Letters*, Vol. 12, 1145–1148, 2013.
24. Kanjanasit, K. and C. Wang, "A high directivity broadband aperture coupled patch antenna using a metamaterial based superstrate," *2012 Loughborough Antennas & Propagation Conference*, 1–4, 2012.
25. Pirhadi, A., M. Hakkak, F. Keshmiri, and R. K. Baee, "Design of compact dual band high directive electromagnetic bandgap (EBG) resonator antenna using artificial magnetic conductor," *IEEE Transactions on Antennas and Propagation*, Vol. 55, No. 6, 1682–1690, Jun. 2007.
26. Ge, Y. and K. P. Esselle, "A resonant cavity antenna based on an optimized thin superstrate," *Microw. Opt. Technol. Lett.*, Vol. 50, No. 12, 3057–3059, Dec. 2008.
27. Sun, Y., Z. N. Chen, Y. Zhang, H. Chen, and T. S. P. See, "Subwavelength substrate-integrated Fabry-Pérot cavity antennas using artificial magnetic conductor," *IEEE Transactions on Antennas and Propagation*, Vol. 60, No. 1, 30–35, Jan. 2012.
28. Feresidis, A. P. and J. C. Vardaxoglou, "High gain planar antenna using optimized partially reflective surfaces," *Proc. Inst. Elect. Eng. Microw. Antennas Propag.*, Vol. 148, No. 6, 345–350, Dec. 2001.
29. Wang, D., W. Che, Y. Chang, K.-S. Chin, and Y. L. Chow, "A low-profile frequency selective surface with controllable triband characteristics," *IEEE Antennas and Wireless Propagation Letters*, Vol. 12, 468–471, 2013.
30. Garg, R., P. Bhartia, I. Bahl, and A. Ittipiboon, *Microstrip Antenna Design Handbook*, Artech House, Norwood, MA, 2001.
31. Wang, S., A. P. Feresidis, G. Goussetis, and J. C. Vardaxoglou, "High gain subwavelength resonant cavity antennas based on metamaterial ground planes," *IEE Proc. Microw. Antennas. Propag.*, Vol. 153, No. 1, 1–6, 2006.